Studies on the Solid Oxide Cell Perovskite Electrode Materials for Soot Oxidation Activity

Chaitra S. Shenoy, Sunaina S. Patil, P. Govardhan, Atmuri Shourya, Hari Prasad Dasari, M. B. Saidutta & Harshini Dasari

Emission Control Science and Technology

ISSN 2199-3629

Emiss. Control Sci. Technol.
DOI 10.1007/s40825-019-00144-z

Emission Control Science and Technology
https://doi.org/10.1007/s40825-019-00144-z

SPECIAL ISSUE: IN RECOGNITION OF PROFESSOR WOLFGANG GRÜNERT'S CONTRIBUTIONS TO THE SCIENCE AND FUNDAMENTALS OF SELECTIVE CATALYTIC REDUCTION OF NOX

Check for updates

Studies on the Solid Oxide Cell Perovskite Electrode Materials for Soot Oxidation Activity

Chaitra S. Shenoy[1] · Sunaina S. Patil[1] · P. Govardhan[1] · Atmuri Shourya[1] · Hari Prasad Dasari[1] · M. B. Saidutta[1] · Harshini Dasari[2]

Received: 17 July 2019 / Revised: 17 September 2019 / Accepted: 24 September 2019

Abstract
Solid oxide cell (SOC) perovskite electrode materials (BSCF ($Ba_{0.5}Sr_{0.5}Co_{0.8}Fe_{0.2}O_{3-\delta}$), LSCF ($La_{0.6}Sr_{0.4}Co_{0.2}Fe_{0.8}O_{3-\delta}$) and LSCM ($La_{0.75}Sr_{0.25}Cr_{0.5}Mn_{0.5}O_{3-\delta}$)) were synthesised using microwave-assisted reverse-strike co-precipitation method and tested for soot oxidation activity. The calcined perovskite materials were characterized using FT-IR, XRD, SEM and BSE, BET and BJH and XPS analysis. The mean activation energy for soot oxidation was calculated from Ozawa plots at various heating rates (5, 10, 15 and 20 K/min) at different levels of soot conversions (T_{10} to T_{90}) for BSCF, LSCM and LSCF perovskite materials and was around 133 ± 11.5, 138 ± 9.9 and 152 ± 7.2 kJ/mol, respectively. Irrespective of the heating rates, BSCF material showed the lowest T_{50} temperature than compared to other samples, and it is correlated to the presence of Fe_3O_4 as a secondary phase.

Keywords SOC perovskite materials · Soot oxidation activity · Secondary phase-Fe_3O_4 · Activation energy · Ozawa plots

1 Introduction

Solid oxide cells (SOCs) operate in electrolyser and fuel cell modes and provide effective conversion of electricity into renewable fuels and vice versa, respectively [1–3]. The most common perovskite material as oxygen electrode for SOCs is a composite of strontium doped lanthanum magnetite (LSM) [4, 5], lanthanum strontium ferrite (LSF) [6], lanthanum strontium cobaltite (LSCo) [5], lanthanum strontium copper ferrite (LSCuF) [7], lanthanum strontium cobalt ferrite (LSCF) [7, 8], lanthanum strontium cobalt magnetite (LSCM) [9] or barium strontium cobalt ferrite (BSCF) [10]. Oxygen reduction reaction and oxygen evolution reaction, along with mixed ionic and electronic conductivities, play a major role in selecting promising oxygen electrode for the SOCs in fuel cell and electrolyser modes [11]. Similarly, the soot oxidation activity in a diesel particulate filter (DPF) works on the active oxygen mechanism in the absence of NO_2 indicating that, in the oxygen-rich gas stream, the DPF catalyst exchanges its oxygen with gas phase oxygen leading to the formation of highly reactive oxygen species which participates in soot oxidation at catalyst-soot interface [12]. Accumulation of soot in DPF results in backpressure and reduces the engine performance in the long run, therefore needs continuous regeneration [13]. Consequently, different measures have to be taken to eliminate soot from the engine exhaust. Only modifying the engine design will not accomplish this, efforts have to be taken to come up with novel catalysts that will help in oxidising soot at lower temperatures (423–673 K) than the temperature at which soot actually oxidises in the air (773–873 K) [14, 15]. Catalytic conversion of soot in a diesel particulate filter (DPF) is one of the promising ways to eliminate soot from a diesel engine exhaust.

The catalysts that are used for oxidation of soot include transition metal oxides [16], alkali and alkaline-earth containing catalysts [17], noble metals [18, 19], perovskites [20], spinel oxides [14] and pure and doped cerium oxides [21].

Electronic supplementary material The online version of this article (https://doi.org/10.1007/s40825-019-00144-z) contains supplementary material, which is available to authorized users.

✉ Hari Prasad Dasari
energyhari@nitk.edu.in

[1] Chemical Engineering Department, National Institute of Technology Karnataka, Mangalore 575025, India

[2] Chemical Engineering Department, Manipal Institute Technology, Manipal Academy of Higher Education (MAHE), Manipal 576104, India

Published online: 21 October 2019

Noble metals like platinum, palladium and rhodium are most widely used catalysts for the same, but they are costly, scarce and cannot withstand high temperatures as they get deactivated due to sintering [14, 22, 23].

In recent years, the perovskite family has garnered a lot of interest in the field of catalysis, due to their physical and chemical properties. These perovskites having ABO_3 structure, where A-site is usually occupied by lanthanides or alkaline-earth metals, B-site is occupied by transition metals and O is oxygen, find applications in several oxidation reactions like CO [24] and hydrocarbon oxidation [25], photocatalysis [26], materials for chemical sensors [27, 28], hydrogenation [29] and hydrogenolysis reactions [30], pollution abatement and electrocatalysis [31]. Partial substitution of cations in A-site and B-site leads to substituted compounds with the formula $A_{1-x}A_xB_{1-y}B_yO_{3-\delta}$. They are also stable at high temperatures (above 1273 K) and are cheaper as compared to noble metals [31–33]. Peron et al. [34] studied two lanthanum-based perovskites ($LaCrO_3$ and $LaMnO_3$) as possible substitutes for noble metal catalysts in the automotive exhaust, along with the substitution of La with K doping in order to increase the catalytic activity. It was found that doping with K led to improved catalytic activity due to the increase in surface oxygen vacancies created by the presence of adsorbed oxygen species. $La_{1-x}K_xCo_{1-y}Cu_yO_{3-\delta}$ perovskites were tested by Li et al. [35] for simultaneous oxidation of soot and NO_x, which showed that the redox properties improved on dual substitution of K and Cu in the $LaCoO_3$ lattice structure, mainly due to change in the oxidation states (by substituting La^{3+} by K^+ and Co^{3+} by Cu^{2+}), which leads to creation of oxygen vacancies, which further increases the surface adsorbed oxygen species (O_2^- and O^-), leading to increased catalytic activity.

The method of synthesis of perovskites is an important factor which defines their physical property, and various synthesis methods were used for preparation of perovskites which includes sol-gel method [18], freeze-drying method, spray-drying method [36], co-precipitation method [37], complexation method [38], hydrothermal method and microwave-assisted methods [39]. Microwave-assisted processes consume lesser energy, are fast and are shown to produce particles having smaller grain size [40]. In this context, an attempt is made to study and understand the suitability of SOC perovskite oxygen electrode materials (BSCF, LSCM and LSCF) for soot oxidation activity, synthesised by microwave-assisted reverse-strike co-precipitation method.

2 Experimental Details

2.1 Material Synthesis

The three perovskites, BSCF ($Ba_{0.5}Sr_{0.5}Co_{0.8}Fe_{0.2}O_{3-\delta}$), LSCF ($La_{0.6}Sr_{0.4}Co_{0.2}Fe_{0.8}O_{3-\delta}$) and LSCM ($La_{0.75}Sr_{0.25}Cr_{0.5}Mn_{0.5}O_{3-\delta}$)), were synthesized by microwave-assisted reverse-strike co-precipitation method, using AR grade chemicals. The metal nitrates used for the same include lanthanum (III) nitrate hexahydrate [$La(NO_3)_3.6H_2O$] (purity ≥ 99%) (Sigma–Aldrich), iron (III) nitrate nonahydrate [$Fe(NO_3)_3.9H_2O$] (purity ≥ 98%) (Sigma–Aldrich), strontium nitrate anhydrous [$Sr(NO_3)_2$] (purity ≥ 99%) (Molychem), cobalt (II) nitrate hexahydrate [$Co(NO_3)_2.6H_2O$] (purity ≥ 98%) (Sigma–Aldrich), barium nitrate [$Ba(NO_3)_2$] (purity ≥ 98.5%) (Loba Chemie), chromium (III) nitrate nonahydrate [$Cr(NO_3)_3.9H_2O$] (purity ≥ 99%) (Sigma–Aldrich), manganese (II) nitrate tetrahydrate [$Mn(NO_3)_2.4H_2O$] (purity ≥ 97%) (Sigma–Aldrich).

In this method, the metal nitrate solution was prepared by dissolving stoichiometric amounts of nitrates in water (used as a solvent). This metal nitrate solution and the ammonium hydroxide assay was added simultaneously and dropwise to water at pH 11 (adjusted by the addition of ammonium hydroxide), and overall pH is maintained at 9 under continuous stirring [41]. The obtained precipitate is allowed to settle overnight, followed by heating the solution in a microwave at 423 K for 30 min (540 W). This allows the particles to heat quickly and leads to lesser clustering of particles [40]. This solution is dried in a hot air oven at 453 K for 24 h. The solid powder is crushed and calcined at 873 K for 5 h (to ensure removal of impurities) in a muffle furnace, and the powder is further re-calcined at 1373 K for 5 h (to ensure proper phase formation) to obtain the desired material.

2.2 Material Characterization

The perovskite materials were analysed using Fourier-transform infra-red spectroscopy (FT-IR) (Bruker Alpha), X-ray diffraction (XRD) (Rigaku Miniflex 6000), scanning electron microscopy (SEM) and back-scattered electron (BSE) (JSM 6380LA), BET surface area and BJH analysis (Quanta Chrome Novae-2200) and X-ray photoelectron spectroscopy (XPS) (Omicron ESCA+). CasaXPS software is used for curve fitting from raw data, using C 1 s peak as a reference, having binding energy 284.6 eV. The peak analysis is obtained using a Shirley background and Gaussian-Lorentzian peak fitting.

2.3 Soot Oxidation Activity

Soot oxidation activity studies were carried out using thermogravimetric analysis (TGA, TG-DTA 6300). Before the soot oxidation experiments, the TGA setup is optimized to eliminate the possible heat and mass transfer effects [42]. Soot (Printex-U, Orion Engineered Chemicals) is used, and the soot to catalyst weight ratio is 1: 10 under tight contact mode. TGA instrument is operated in the temperature range of 473 to

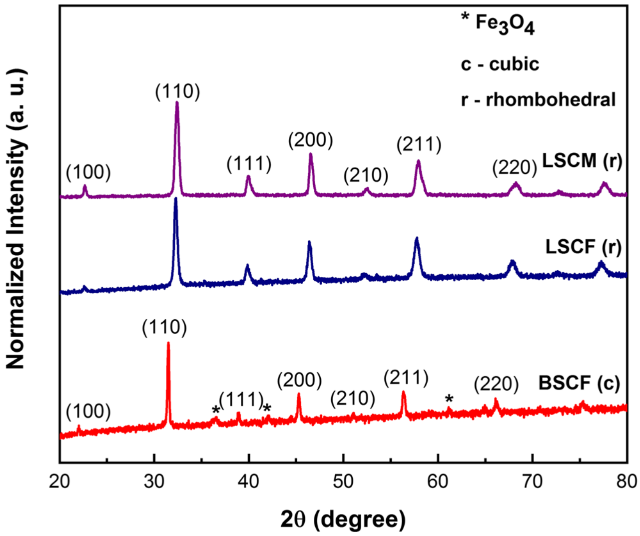

Fig. 1 XRD patterns of the BSCF, LSCM and LSCF perovskite materials synthesised by microwave-assisted reverse-strike co-precipitation method, calcined at 1373 K/5 h

873 K at various heating rates (5, 10, 15 and 20 K/min) in an air atmosphere at a flow rate of 100 ml/min.

The apparent activation energy for soot oxidation is obtained using the following expression determined by Ozawa method, given as [13, 43–45]:

$$[d(\log(\phi))]/[d(1/T_\alpha)] = -0.4567E_a/R \quad (1.1)$$

where ϕ is the heating rate (K/min) (ϕ = 5, 10, 15 and 20 K/min), T_α is the temperature corresponding to $\alpha\%$ ($\alpha\%$ = 10, 20, 30, 40, 50, 60, 70, 80 and 90%) carbon conversion, E_a is the apparent activation energy (kJ/mol) and R is the ideal gas constant (= 8.314 J/ (mol K)). Using the least squares straight-line fit, E_a can be estimated from the slope of log (ϕ) versus ($1/T_\alpha$) plot.

3 Results and Discussion

3.1 Material Characterization

Figure S1 (*Supplementary Information*) depicts the FT-IR spectra of the perovskite materials calcined at 1373 K/5 h in air and shows the formation of the metal oxygen bonds in all the materials. Figure 1 shows the XRD patterns of BSCF, LSCM and LSCF materials. For BSCF, LSCF and LSCM materials, major diffraction peaks (100), (110), (111), (200), (210), (211) and (220) correspond to the cubic perovskite phase of BSCF [46, 47], the rhombohedral phase of LSCF [48, 49] and the rhombohedral phase of LSCM [50–52], respectively. For BSCF material, in addition to the major peaks, low-intensity peaks were observed at 2θ = 36.52°, 42.09°, and 61.08°, which were identified as Fe_3O_4 [53, 54]. It indicates that a secondary phase (Fe_3O_4) is formed, along with the BSCF phase. No visible secondary phase formation or peak shift can be identified in the LSCF and LSCM perovskites materials, indicating pure phase formation [55, 56].

Table 1 shows the physiochemical properties obtained from XRD, BET and BJH analysis. The crystallite size and lattice strain for the BSCF, LSCF and LSCM perovskite materials from XRD data are around 41, 19 and 19 nm and 0.0023, 0.0052 and 0.0054, respectively. The BET surface area and pore volume of BSCF, LSCF and LSCM perovskite materials obtained from BET and BJH analysis are around 20, 39 and 4 m^2/g and 0.036, 0.059 and 0.004 cc/g, respectively. Fig. S2 (*Supplementary Information*) shows the N_2 adsorption-desorption isotherms and pore size distribution of the perovskite materials. Type IV adsorption isotherm with H3 type hysteresis loop is obtained indicating the dependency of isotherm on the quality/surface of the porous solid perovskite materials having slit-shaped pores of non-uniform size and shape. From the BJH pore size distribution, all the perovskite materials displayed a mesoporous structure having a pore size ranging from 2 to 50 nm.

Figure 2 depicts the SEM and BSE images of the perovskite materials. The SEM images show that the obtained materials are agglomerated. The agglomerate size of the BSCF and LSCF perovskite materials is around 20 to 25 μm, and for the LSCM material, it is less than 5 μm. Compared with the crystallite size obtained from the XRD data, BSCF and LSCF materials displayed a higher degree of agglomeration than LSCM material. BSE analysis is carried out to find out the presence of any secondary phase in the perovskite materials. From a close observation, BSCF material showed a variation in colour, but this variation cannot be attributed to the secondary phase since such variation is also possible due to topography changes. LSCM and LSCF have not shown major colour variations.

Figure 3 represents the XPS spectra of BSCF (Fig. 3a), LSCF (Fig. 3b) and LSCM (Fig. 3c) perovskites. The

Table 1 Crystallite size, lattice strain, BET surface area and pore volume of BSCF, LSCF and LSCM perovskite materials, calcined at 1373 K/5 h, obtained from XRD, BET and BJH analysis

Perovskites	Crystallite size[a] (nm)	Lattice strain[b]	BET surface area (m^2/g)	Pore volume (cc/g)
BSCF	41	0.0023	20	0.036
LSCF	19	0.0052	39	0.059
LSCM	19	0.0054	04	0.004

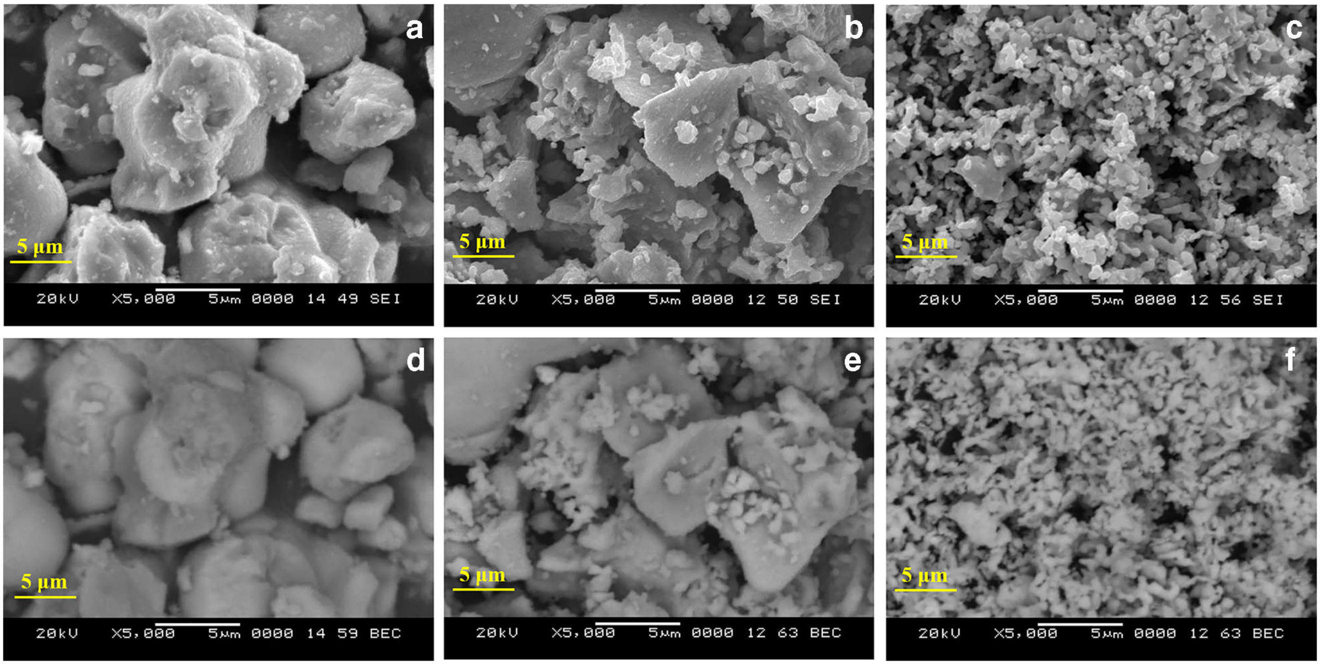

Fig. 2 SEM and BSE images of the BSCF (**a**, **d**), LSCM (**b**, **e**) and LSCF (**c**, **f**) perovskite materials

deconvoluted peaks from obtained XPS data of Ba_{3d}, Sr_{3d}, Co_{2p}, Fe_{2p}, La_{3d}, Cr_{2p} and Mn_{2p} level of the perovskites were analysed, and the oxidation states were assigned accordingly which also matched well with the literature [51, 57–65]. From the Fig. 3a, it is difficult to identify the oxidation state of cobalt due to overlapping of Ba 3d and Co 2p. Figure 4 displays the O1s spectra of all the three perovskites. The spectrum was well fitted into two peaks, and the peak obtained at lower binding energy (528–530 eV) is ascribed to surface lattice oxygen species (O^{2-}), and that of higher binding energy (530.5–532.5 eV) belongs to surface adsorbed oxygen species (O_2^{2-}, O_2^-& O^-) which is due to the presence of carbonate/hydroxyl groups or adsorbed water molecule [66, 67].

The amount of lattice and adsorbed oxygen species are obtained by calculating the ratio of individual oxygen species to the total oxygen species and are tabulated in Table 2. The surface adsorbed oxygen species were found to be high for LSCF and LSCM perovskites than compared to BSCF. From Table 2, it can also be seen that the amount of lattice oxygen ($O_{lattice}$/ O_{total}) is high for BSCF perovskites. From the work carried out by Urasaki et al. [68], Ming et al. [69], Chen et al. [70] and Grimaudet al. [71], it was reported that the surface lattice oxygen also favours the catalytic activity. However, the catalytic stability and activity are associated closely with the transfer of bulk lattice oxygen to fill the surface lattice oxygen also [70]. Apart from that, the involvement of lattice oxygen species in the oxidation reactions is more versatile than gaseous oxygen as it decreases the vacancy formation energy and eases diffusion in the material [72].

3.2 Soot Oxidation Activity Studies

Figure 5 shows the soot oxidation conversion obtained for BSCF, LSCF and LSCM perovskite materials with an increase in the temperature at a heating rate of 10 K/min. Sigmoidal-shaped curves were obtained and BSCF material showed a better T_{50} temperature (734 K) than compared to LSCM (747 K) and LSCF (773 K) materials. When compared to ceria-based catalysts [73–75], the soot oxidation activity of the SOC perovskites is less and it can be due to high calcination temperature of perovskites. Nevertheless, efforts have to be made to decrease the heat treatment temperature at which these SOC perovskite structures are formed. When compared to single redox oxides (CeO_2, SnO_2, Pr_6O_{11} and Mn_3O_4) and non-redox oxides (Gd_2O_3, La_2O_3, ZrO_2, and HfO_2), the BSCF perovskite showed better T_{50} (734 K) [76]. Figure 6 demonstrates the soot oxidation conversion obtained for BSCF (Fig. 6a), LSCF (Fig. 6b) and LSCM (Fig. 6c) materials with the increase in the temperature at various heating rates (5, 10, 15 and 20 K/min) and sigmoidal-shaped curves were obtained. Irrespective of the tested perovskite, material dependence of the soot conversion on the heating rate is noticed and soot conversion is shifted to higher temperatures with the increase of heating rates from 5 to 20 K/min. To further understand the phenomena and to obtained the activation energy for the perovskite materials, Ozawa plots at various soot conversions (α = 10 to 90%)) were obtained from Fig. 6 and depicted in Fig. 7. From Fig. 7, a family of straight and parallel lines is obtained for all the materials at the same degree of soot

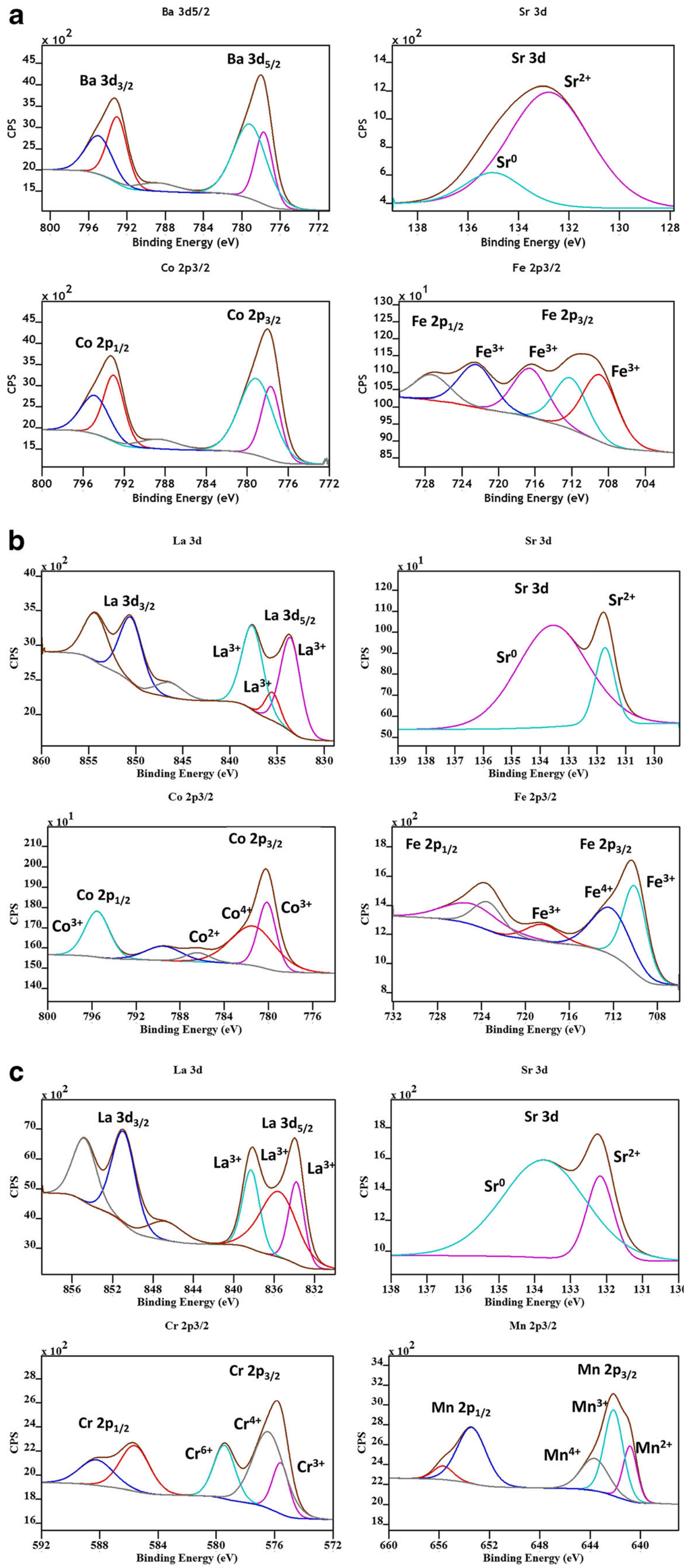

Fig. 3 XPS analysis of the BSCF (**a**), LSCF (**b**) and LSCM (**c**) perovskites with the corresponding metal oxidation states

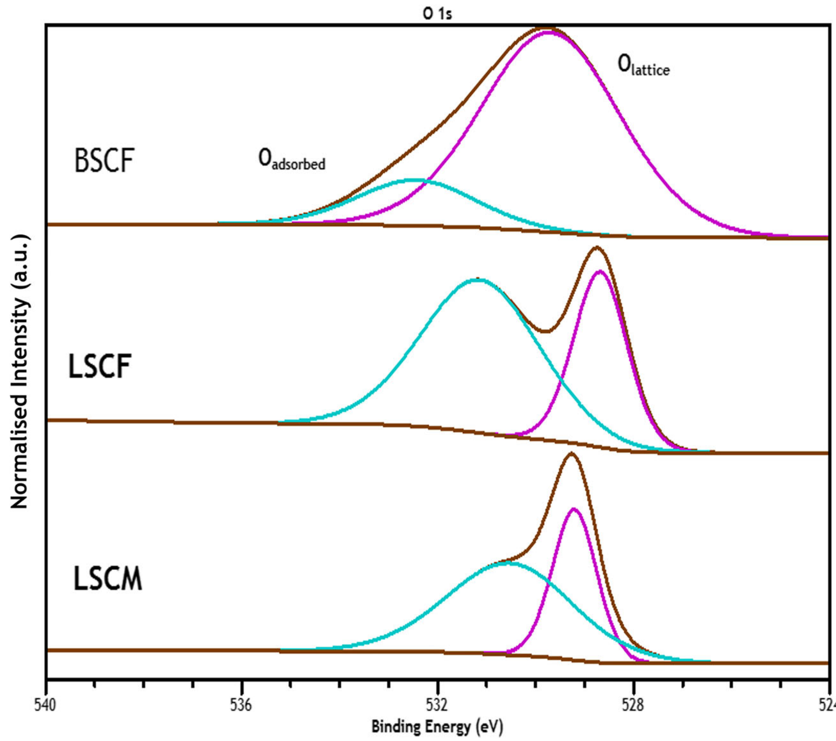

Fig. 4 O 1s spectra of the BSCF, LSCF and LSCM perovskites

conversion and the activation energy for each conversion line can be obtained from its slope. Activation energy hardly varied with the extent of conversion for the perovskite materials indicating a single-step reaction. A mean value of 133 ± 11.5 kJ/mol, 138 ± 9.9 kJ/mol and 152 ± 7.2 kJ/mol is calculated and reported as apparent activation energy of the soot oxidation process for the BSCF, LSCM and LSCF perovskite materials respectively and is lower than the activation energy (168 kJ/mol) of uncatalyzed soot oxidation [77]. The presence of secondary phase (Fe_3O_4) in BSCF material could be one of the reasons for the better soot oxidation performance than compared to other perovskite materials. From XRD data (Fig. 1), it is evidenced that the BSCF material has Fe_3O_4 as a secondary phase. From the literature [78, 79], the temperature programmed reduction (TPR) profiles of bulk Fe_2O_3, the reduction of Fe_3O_4 to Fe is noticed in the range of ~ 903 to 943 K. This indicates that the secondary phase (Fe_3O_4) benefits the soot oxidation owing to presence of iron in mixed oxidation states (Fe^{2+}/Fe^{3+}) and promotes soot oxidation at lower temperatures in BSCF material than compared to other perovskite materials. The present study indicates the possibility of the application of SOC perovskite oxygen electrode materials as catalysts for soot oxidation in diesel particulate filters.

Wagloehner et al. [80, 81] have studied the transport of oxygen from iron oxide catalysts to the soot surface during soot oxidation. The contact points between soot and catalyst lead to generation of surface oxygen vacancies due to transfer of oxygen from the bulk of the catalyst to its surface, which was understood using isotopic TPO studies. This transfer of oxygen to soot leads to reduction of iron oxide to active iron species. The surface oxygen vacancies were replenished by either diffusion of bulk oxygen (movement through lattice vacancies) or gas phase oxygen and the bulk oxygen

Table 2 O 1s data of BSCF, LSCF and LSCM perovskite materials, calcined at 1373 K/5 h, obtained from XPS analysis

Sample	Secondary phase[a] (XRD)	B.E eV ($O_{lattice}$)	B.E eV ($O_{adsorbed}$)	$O_{lattice}/O_{total}$	$O_{adsorbed}/O_{total}$	T_{10} (K) [b]	T_{50} (K) [b]	T_{90} (K) [b]
BSCF	Fe_3O_4	529.7	532.4	0.83	0.16	652	734	780
LSCF	–	528.6	531.1	0.28	0.71	692	773	815
LSCM	–	529.2	530.5	0.36	0.63	682	747	774

[a] From XRD data

[b] From Fig. 5 data

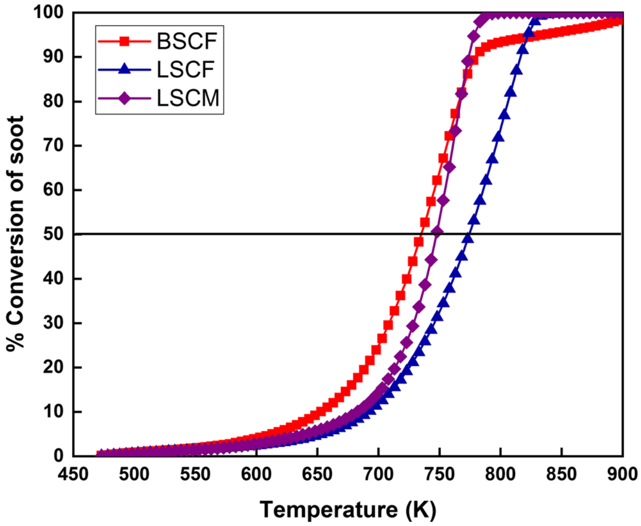

Fig. 5 Soot oxidation conversion of the BSCF, LSCF and LSCM perovskite materials with an increase of temperature at a heating rate of 10 K/min

replenished vacancies by relocation of surface oxygen to bulk. This might be a possible reaction mechanism, which clarifies the reason for lower soot oxidation temperature of BSCF, mainly due to the presence of Fe_3O_4, which has higher amount of bulk/lattice oxygen as compared to LSCF and LSCM.

4 Conclusion

Microwave-assisted reverse-strike co-precipitation method is used for the synthesis of SOC perovskite oxygen electrode (BSCF, LSCF and LSCM) materials, and the calcined samples were characterized by XRD, SEM and XPS analysis and tested for soot oxidation activity. From XRD analysis, BSCF perovskite materials displayed a cubic structure along with a secondary phase formation of Fe_3O_4, LSCM and LSCF perovskite materials showed a rhombohedral structure. The soot oxidation activity studies showed that BSCF sample showed better activity as compared to LSCM and LSCF samples. The mean activation energies for the soot oxidation process, calculated using Ozawa plots, are 133 ± 11.5 kJ/mol, 138 ± 9.9 kJ/mol and 152 ± 7.2 kJ/mol for BSCF, LSCM and LSCF samples respectively. Formation of secondary phase (Fe_3O_4) in BSCF sample promoted a positive effect on soot oxidation activity, due to lattice/bulk oxygen vacancy.

Acknowledgements We acknowledge MRC, MNIT Jaipur for facilitating XPS data and MARC-BIT, Bangalore, for BET surface area and BJH data.

Funding Information SERB-IMPRINT-II Project "Development and demonstration of solid oxide electrolysis technology for co-electrolysis of CO_2 and H_2O for the production of syngas" (IMP/2018/1318/AM) funded this work. Prof. M B Saidutta and Dr. Hari Prasad Dasari thank

Fig. 6 Soot oxidation conversion of BSCF (**a**), LSCF (**b**) and LSCM (**c**) perovskite materials with an increase of temperature at a heating rate of 5, 10, 15 and 20 K/min

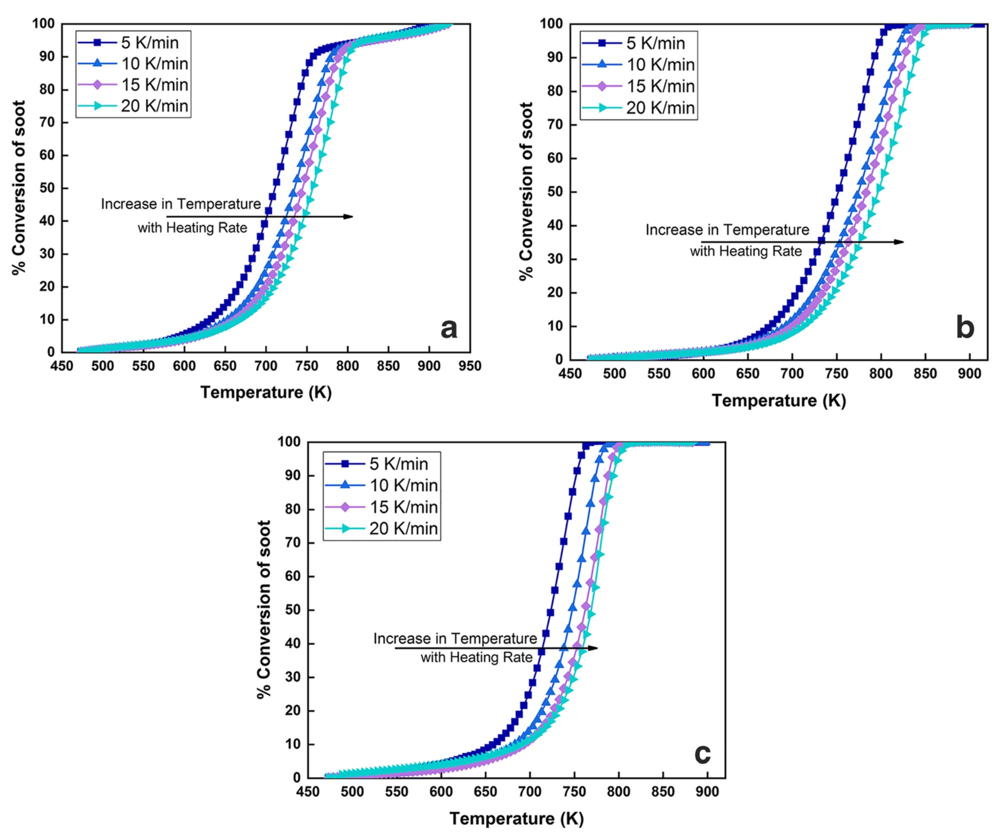

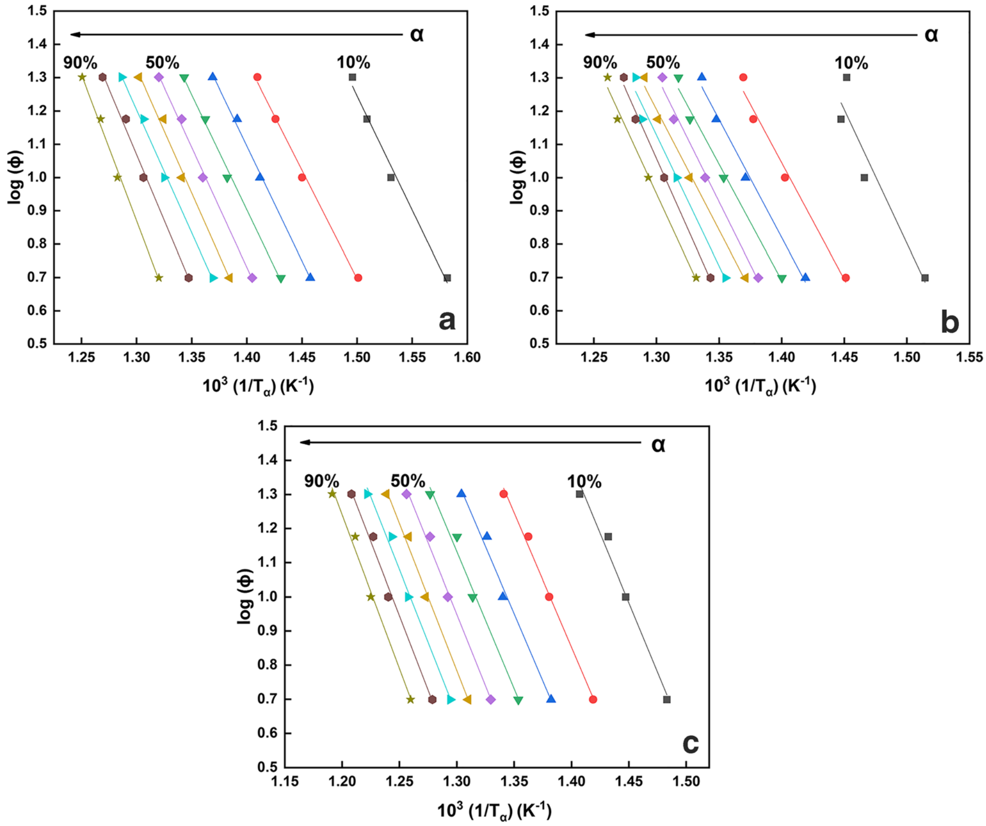

Fig. 7 Ozawa plots of BSCF (**a**), LSCF (**b**) and LSCM (**c**) perovskite materials obtained from Fig. 6 data

Indo-US Twenty-First Century Knowledge Initiative program grant on "Methanol as a clean energy source for India" received from UGC.

Compliance with Ethical Standards

Competing Interests The authors declare that they have no competing interests.

References

1. Bierschenk, D.M., Wilson, J.R., Barnett, S.A.: High efficiency electrical energy storage using a methane-oxygen solid oxide cell. Energy Environ. Sci. **4**, 944–951 (2011). https://doi.org/10.1039/c0ee00457j
2. Jensen, S.H., Graves, C., Mogensen, M., Wendel, C., Braun, R., Hughes, G., Gao, Z., Barnett, S.A.: Large-scale electricity storage utilizing reversible solid oxide cells combined with underground storage of CO_2 and CH_4. Energy Environ. Sci. **8**, 2471–2479 (2015). https://doi.org/10.1039/c5ee01485a
3. Laguna-Bercero, M.A., Kilner, J.A., Skinner, S.J.: Development of oxygen electrodes for reversible solid oxide fuel cells with scandia stabilized zirconia electrolytes. Solid State Ionics. **1**, 501–504 (2011). https://doi.org/10.1016/j.ssi.2010.01.003
4. O'Brien, J.E., Stoots, C.M., Herring, J.S., Hartvigsen, J.: Hydrogen production performance of a 10-cell planar solid-oxide electrolysis stack. J. Fuel Cell. Sci. Technol. **3**, 213–219 (2006). https://doi.org/10.1115/1.2179435
5. Wang, W., Huang, Y., Jung, S., Vohs, J.M., Gorte, R.J.: A comparison of LSM, LSF, and LSCo for solid oxide electrolyzer anodes. J. Electrochem. Soc. **11**, A2066–A2070 (2006). https://doi.org/10.1149/1.2345583
6. Jensen, S.H., Larsen, P.H., Mogensen, M.: Hydrogen and synthetic fuel production from renewable energy sources. Int. J. Hydrog. Energy. **32**, 3253–3257 (2007). https://doi.org/10.1016/j.ijhydene.2007.04.042
7. Marina, O.A., Pederson, L.R., Williams, M.C., Coffey, G.W., Meinhardt, K.D., Nguyen, C.D., Thomsen, E.C.: Electrode performance in reversible solid oxide fuel cells. J. Electrochem. Soc. **154**, B452–B459 (2007). https://doi.org/10.1149/1.2710209
8. Schiller, G., Ansar, A., Lang, M., Patz, O.: High temperature water electrolysis using metal supported solid oxide electrolyser cells (SOEC). J. Appl. Electrochem. **39**(2), 293–301 (2009). https://doi.org/10.1007/s10800-008-9672-6
9. Yang, X., Irvine, J.T.S.: $(La_{0.75}Sr_{0.25})_{0.95}Mn_{0.5}Cr_{0.5}O_3$ as the cathode of solid oxide electrolysis cells for high temperature hydrogen production from steam. J. Mater. Chem. **18**, 2349–2354 (2008). https://doi.org/10.1039/b800163d
10. Kriegel, R., Kircheisen, R., Töpfer, J.: Oxygen stoichiometry and expansion behavior of $Ba_{0.5}Sr_{0.5}Co_{0.8}Fe_{0.2}O_{3-δ}$. Solid State Ionics. **181**, 64–70 (2010). https://doi.org/10.1016/j.ssi.2009.11.012
11. Wei, B., Chen, K., Wang, C.C., Lü, Z., Jiang, S.P.: Cr deposition on porous $La_{0.6}Sr_{0.4}Co_{0.2}Fe_{0.8}O_{3-δ}$ electrodes of solid oxide cells under open circuit condition. Solid State Ionics. **281**, 29–37 (2015). https://doi.org/10.1016/j.ssi.2015.08.018
12. Mukherjee, D., Rao, B.G., Reddy, B.M.: CO and soot oxidation activity of doped ceria: influence of dopants. Appl. Catal. B Environ. **197**, 105–115 (2016). https://doi.org/10.1016/j.apcatb.2016.03.042
13. Russo, N., Fino, D., Saracco, G., Specchia, V.: Studies on the redox properties of chromite perovskite catalysts for soot combustion. J.

Catal. **229**, 459–469 (2005). https://doi.org/10.1016/J.JCAT.2004.11.025

14. Liu, H., Dai, X., Wang, K., Yan, Z., Qian, L.: Highly efficient catalysts of $Mn_{1-x}Ag_xCo_2O_4$ spinel oxide for soot combustion. Catal. Commun. **101**, 134–137 (2017)
15. Feng, N., Wu, Y., Meng, J., Chen, C., Wang, L., Wan, H., Guan, G.: Catalytic combustion of soot over Ce and co substituted three-dimensionally ordered macroporous $La_{1-x}Ce_xFe_{1-y}Co_yO_3$ perovskite catalysts. RSC Adv. **5**, 91609–91618 (2015)
16. Neelapala, S.D., Shetty, A., Gaggar, G., Mall, R., Dasari, H.: Development of iron doped manganese oxide (Mn_{2-x} Fe_x O_3) catalysts for soot oxidation applications. Int. J. Appl. Eng. Res. **13**, 245–251 (2018)
17. Weng, D., Li, J., Wu, X., Si, Z.: Modification of CeO_2-ZrO_2 catalyst by potassium for NOx-assisted soot oxidation. J. Environ. Sci. **23**, 145–150 (2011)
18. Da, Y., Zeng, L., Wang, C., Mao, T., Chen, R., Gong, C., Fan, G.: Catalytic oxidation of diesel soot particulates over Pt substituted $LaMn_{1-x}Pt_xO_3$ perovskite oxides. Catal. Today. **327**, 73–80 (2018). https://doi.org/10.1016/j.cattod.2018.06.007
19. Liu, S., Wu, X., Liu, W., Chen, W., Ran, R., Li, M., Weng, D.: Soot oxidation over CeO_2 and Ag/CeO_2: factors determining the catalyst activity and stability during reaction. J. Catal. **337**, 188–198 (2016). https://doi.org/10.1016/j.jcat.2016.01.019
20. Lopez-Suarez, F.E., Parres-Esclapez, A., Bueno-López, M.J., Illán-Gómez, B., Ura, J.: Trawczyński, role of surface and lattice copper species in copper-containing (mg / Sr) TiO_3 perovskite catalysts for soot combustion. Appl. Catal. B Environ. **93**, 82–89 (2009). https://doi.org/10.1016/j.apcatb.2009.09.015
21. Bueno-López, A.: Diesel soot combustion ceria catalysts. Appl. Catal. B Environ. **146**, 1–11 (2014). https://doi.org/10.1016/j.apcatb.2013.02.033
22. Sudarsanam, P., Kuntaiah, K., Reddy, B.M.: Promising ceria-samaria-based nano-oxides for low tempearature soot oxidation: a combined study of structure-activity properties. New J. Chem. **38**, 5991–6001 (2014). https://doi.org/10.1039/C4NJ01274G
23. Katta, L., Sudarsanam, P., Thrimurthulu, G., Reddy, B.M.: Doped nanosized ceria solid solutions for low temperature soot oxidation : zirconium versus lanthanum promoters. Appl. Catal. B Environ. **101**, 101–108 (2010). https://doi.org/10.1016/j.apcatb.2010.09.012
24. Wang, X., Huang, K., Yuan, L., Xi, S., Yan, W., Geng, Z., Cong, Y., Sun, Y., Tan, H., Wu, X., Li, L., Feng, S.: Activation of surface oxygen sites in a cobalt-based perovskite model catalyst for CO oxidation. J. Phys. Chem. Lett. **9**, 4146–4154 (2018). https://doi.org/10.1021/acs.jpclett.8b01623
25. Miller, J.E., Sault, A.G., Trudell, D.E., Nenoff, T.M., Thoma, S.G., Jackson, N.B.: Oxidation reactions of ethane over Ba-Ce-O based perovskites. Appl. Catal. A Gen. 45–54 (2000). https://doi.org/10.1016/S0926-860X(00)00429-4
26. Xu, Y., Yang, M., Chen, B., Wang, X., Chen, H., Kuang, D., Su, C.: A $CsPbBr_3$ perovskite quantum dot/graphene oxide composite for photocatalytic CO 2 reduction. J. Am. Chem. Soc. **139**, 5660–5663 (2017). https://doi.org/10.1021/jacs.7b00489
27. Stoeckel, M., Gobbi, M., Bonacchi, S., Liscio, F., Ferlauto, L., Orgiu, E., Samorì, P.: Reversible, fast, and wide-range oxygen sensor based on nanostructured organometal halide perovskite. Adv. Mater. **29**, 1–7 (2017). https://doi.org/10.1002/adma.201702469
28. Aamir, M., Khan, D., Sher, M., Bhosale, S.V., Malik, M., Akhtar, J., Revaprasadu, N.: A facile route to cesium lead bromoiodide perovskite microcrystals and their potential application as sensors for nitrophenol explosives. Eur. J. Inorg. Chem. 3755–3760 (2017). https://doi.org/10.1002/ejic.201700660
29. Hus, M., Kopac, D., Likozar, B.: Catalytic hydrogenation of carbon dioxide to methanol: synergistic effect of bifunctional Cu/perovskite catalysts. ACS Catal. **9**, 105–116 (2019). https://doi.org/10.1021/acscatal.8b03810
30. Gao, F., Liu, H., Hu, X., Chen, J., Zhiwei, H., Xia, C.: Selective hydrogenolysis of furfuryl alcohol to 1,5- and 1,2-pentanediol over Cu-LaCoO3 catalysts with balanced Cu0-CoO sites. Chin. J. Catal. **39**, 1711–1723 (2018)
31. Fierro, J.L.G., Pena, M.A.: Chemical structures and performance of perovskite oxides. Chem. Rev. **101**, 1981–2017 (2001)
32. Zhu, J., Thomas, A.: Perovskite-type mixed oxides as catalytic material for NO removal. Appl. Catal. B Environ. **92**, 225–233 (2009). https://doi.org/10.1016/j.apcatb.2009.08.008
33. Fino, D., Bensaid, S., Piumetti, M., Russo, N.: A review on the catalytic combustion of soot in diesel particulate filters for automotive applications: from powder catalysts to structured reactors. Appl. Catal. A Gen. **509**, 75–96 (2016)
34. Peron, G., Glisenti, A.: Perovskites as alternatives to noble metals in automotive exhaust abatement: activation of oxygen on $LaCrO_3$ and $LaMnO_3$. Top. Catal. **62**(1-4), 244–251 (2018). https://doi.org/10.1007/s11244-018-1120-1
35. Li, Z., Meng, M., Zha, Y., Dai, F., Hu, T., Xie, Y., Zhang, J.: Highly efficient multifunctional dually-substituted perovskite catalysts $La_{1-x}K_xCo_{1-y}Cu_yO_{3-\delta}$ used for soot combustion, NOx storage and simultaneous NOx-soot removal. Appl. Catal. B Environ. **121–122**, 65–74 (2012). https://doi.org/10.1016/j.apcatb.2012.03.022
36. Atta, N.F., Galal, A., El-Ads, E.H.: Perovskite nanomaterials—synthesis, characterization, and applications, Chapter 4, pp. 107–151. IntechOpen (2015) https://doi.org/10.5772/61280
37. Labhsetwar, N.K., Dhakad, M., Rayalu, S.S., Kumar, R., Subrt, J., Haneda, H., Devotta, S., Mitsuhashi, T.: Thermally stable metal ruthenate based soot oxidation catalyst for diesel exhaust emission control. Top. Catal. **42–43**(1-4), 299–302 (2007). https://doi.org/10.1007/s11244-007-0195-x
38. Patra, H., Rout, S.K., Pratihar, S.K., Bhattacharya, S.: Effect of process parameters on combined EDTA—citrate synthesis of $Ba_{0.5}Sr_{0.5}Co_{0.8}Fe_{0.2}O_{3-\delta}$ perovskite. Powder Technol. **209**, 98–104 (2011). https://doi.org/10.1016/j.powtec.2011.02.015
39. Uran, L., Gallego, J., Santamaria, L.W.Y.A.: Effect of catalyst preparation for the simultaneous removal of soot and NO_x. Appl. Catal. A Gen. **569**, 157–169 (2019)
40. Alvarez-Galvan, C., Trunschke, A., Falcon, H., Sanchez-Sanchez, M., Campos-Martin, J.M., Schlogl, R., Fierro, J.L.G.: Microwave-assisted coprecipitation synthesis of $LaCoO_3$ nanoparticles and their catalytic activity for syngas production by partial oxidation of methane. Front Energy Res. **6**, 1–11 (2018)
41. Zampiva, R.Y.S., Acauan, L.H., dos Santos, L.M., de Castro, R.H.R., Alves, A.K., Bergmann, C.P.: Nanoscale synthesis of single-phase forsterite by reverse strike co-precipitation and its high optical and mechanical properties. Ceram. Int. **43**, 16225–16231 (2017)
42. Neeft, J.P.A., Hoornaert, F., Makkee, M., Moulijn, J.A.: The effects of heat and mass transfer in thermogravimetrical analysis. A case study towards the catalytic oxidation of soot. Thermochim. Acta. **287**, 261–278 (1996). https://doi.org/10.1016/S0040-6031(96)03002-X
43. Shimizu, K., Kawachi, H., Satsuma, A.: Study of active sites and mechanism for soot oxidation by silver-loaded ceria catalyst. Appl. Catal. B Environ. **96**, 169–175 (2010). https://doi.org/10.1016/J.APCATB.2010.02.016
44. Krishna, K., Bueno-López, A., Makkee, M., Moulijn, J.A.: Potential rare earth modified CeO_2 catalysts for soot oxidation I. Characterisation and catalytic activity with O_2. Appl. Catal. B Environ. **75**, 189–200 (2007). https://doi.org/10.1016/j.apcatb.2007.04.010
45. Palmisano, P., Russo, N., Fino, P., Fino, D., Badini, C.: High catalytic activity of SCS-synthesized ceria towards diesel soot combustion. Appl. Catal. B Environ. **69**, 85–92 (2006). https://doi.org/10.1016/J.APCATB.2006.06.002
46. Devi, C.S., Prasad, G.: Development of nano-structured and nano-porous BSCF cathode for low temperature solid oxide fuel cell

application. Trans. Indian Ceram. Soc. **77**, 67–72 (2018). https://doi.org/10.1080/0371750X.2018.1452633
47. Chen, D., Shao, Z.: Surface exchange and bulk diffusion properties of Ba0.5Sr0.5Co0.8Fe0.2O3−δ mixed conductor. Int. J. Hydrog. Energy. **36**, 6948–6956 (2011). https://doi.org/10.1016/j.ijhydene.2011.02.087
48. Giuliano, A., Carpanese, M.P., Clematis, D., Boaro, M.: Infiltration, overpotential and ageing effects on cathodes for solid oxide fuel cells : $La_{0.6}Sr_{0.4}Co_{0.2}Fe_{0.8}O_{3-\delta}$ versus $Ba_{0.5}Sr_{0.5}Co_{0.8}Fe_{0.2}O_{3-\delta}$. J. Electrochem. Soc. **164**, F3114–F3122 (2017). https://doi.org/10.1149/2.0161710jes
49. Lee, C., Jeon, Y., Hata, S., Park, J., Akiyoshi, R., Saito, H., Teraoka, Y., Shul, Y., Einaga, H.: Three-dimensional arrangements of perovskite-type oxide nano-fiber webs for effective soot oxidation. Appl. Catal. B Environ. **191**, 157–164 (2016). https://doi.org/10.1016/j.apcatb.2016.03.001
50. Bastidas, D.M., Tao, S., Irvine, J.T.S.: A symmetrical solid oxide fuel cell demonstrating redox stable perovskite electrodes. J. Mater. Chem. **16**, 1603–1605 (2006)
51. Zhang, X., Song, Y., Guan, F., Zhou, Y., Liu, Q., Wang, G., Bao, X.: $(La_{0.75}Sr_{0.25})_{0.95}(Cr_{0.5}Mn_{0.5})O_{3-\delta}$-$Ce_{0.8}Gd_{0.2}O_{1.9}$ scaffolded composite cathode for high temperature CO_2 electroreduction in solid oxide electrolysis cell. J. Power Sources. **400**, 104–113 (2018)
52. Tao, S., Irvine, J.T.S.: Synthesis and characterization of $(La_{0.75}Sr_{0.25})Cr_{0.5}Mn_{0.5}O_{3-\delta}$, a redox-stable, efficient perovskite anode for SOFCs. J. Electrochem. Soc. **151**, A252–A259 (2004)
53. Rusianto, T., Wildan, M.W., Abraha, K.: Kusmono, various sizes of the synthesized Fe_3O_4 nanoparticles assisted by mechanical vibrations. Indian J. Eng. Mater. Sci. **22**, 175–180 (2015)
54. Legutko, P., Kaspera, W., Stelmachowski, P., Sojka, Z., Kotarba, A.: Boosting the catalytic activity of magnetite in soot oxidation by surface alkali promotion. Catal. Commun. **54**, 139–142 (2014). https://doi.org/10.1016/j.catcom.2014.07.020
55. dos Santos-Gómez, L., Porras-Vázquez, J.M., Losilla, E.R., Martín, F., Ramos-Barrado, J.R., Marrero-López, D.: LSCF-CGO nanocomposite cathodes deposited in a single step by spray-pyrolysis. J. Eur. Ceram. Soc. **38**, 1647–1653 (2018). https://doi.org/10.1016/j.jeurceramsoc.2017.10.010
56. Chanquı, C.M., Vega-Castillo, J.E., Soldati, A.L., Troiani, H., Caneiro, A.: Synthesis and characterization of pure-phase $La_{0.75}Sr_{0.25}Cr_{0.5}Mn_{0.5}O_3$ 2d nanocrystallites for solid oxide fuel cell applications. 14, J Nanopart Res 1–14 (2012). https://doi.org/10.1007/s11051-012-1104-1
57. Mao, L., Zhao, X., Xiao, Y., Dong, G.: The effect of the structure and oxygen defects on the simultaneous removal of NO x and soot by $La_{2-x}Ba_xCuO_4$. New J. Chem. **43**, 4196–4204 (2019). https://doi.org/10.1039/c8nj04233k
58. Zhou, W., Zhao, M., Liang, F., Smith, S.C., Zhu, Z.: High activity and durability of novel perovskite electrocatalysts for water oxidation. Mater. Horizons. **2**, 495–501 (2015). https://doi.org/10.1039/c5mh00096c
59. Mizokawa, T., Morita, Y., Sudayama, T., Takubo, K., Yamada, I., Azuma, M., Takano, M., Shimakawa, Y.: Metallic versus insulating behavior in the A—site ordered perovskite oxides $ACu_3Co_4O_{12}$ (A=Ca and Y) controlled by Mott and Zhang-Rice physics. Phys. Rev. B - Condens. Matter. Mater. Phys. **80**, 3–6 (2009). https://doi.org/10.1103/PhysRevB.80.125105
60. Prasad, D.H., Park, S.Y., Oh, E.O., Ji, H., Kim, H.R., Yoon, K.J., Son, J.W., Lee, J.H.: Synthesis of nano-crystalline $La_{1-x}Sr_xCoO_{3-\delta}$ perovskite oxides by EDTA-citrate complexing process and its catalytic activity for soot oxidation. Appl. Catal. A Gen. **447–448**, 100–106 (2012). https://doi.org/10.1016/j.apcata.2012.09.008
61. Il Jung, J., Edwards, D.D.: X-ray photoelectron (XPS) and diffuse reflectance infra fourier transformation (DRIFT) study of $Ba_{0.5}Sr_{0.5}Co_xFe_{1-x}O_{3-\delta}$ (BSCF: X=0–0.8) ceramics. J. Solid State Chem. **184**, 2238–2243 (2011). https://doi.org/10.1016/j.jssc.2011.06.016
62. Mickevičius, S., Grebinskij, S., Bondarenka, V., Vengalis, B., Šliužiene, K., Orlowski, B.A., Osinniy, V., Drube, W.: Investigation of epitaxial $LaNiO_{3-x}$ thin films by high-energy XPS. J. Alloys Compd. **423**, 107–111 (2006). https://doi.org/10.1016/j.jallcom.2005.12.038
63. Xu, X., Pan, Y., Zhou, W., Chen, Y., Zhang, Z., Shao, Z.: Toward enhanced oxygen evolution on perovskite oxides synthesized from different approaches: a case study of $Ba_{0.5}Sr_{0.5}Co_{0.8}Fe_{0.2-\delta}$. Electrochim. Acta. **219**, 553–559 (2016)
64. Merino, N.A., Barbero, B.P., Eloy, P., Cadús, L.E.: $La_{1-x}Ca_xCoO_3$ perovskite-type oxides: identification of the surface oxygen species by XPS. Appl. Surf. Sci. **253**, 1489–1493 (2006). https://doi.org/10.1016/j.apsusc.2006.02.035
65. Sutthiumporn, K., Maneerung, T., Kathiraser, Y., Kawi, S.: CO2 dry-reforming of methane over $La_{0.8}Sr_{0.2}Ni_{0.8}M_{0.2}O_3$ perovskite (M = Bi, Co, Cr, Cu, Fe): roles of lattice oxygen on C-H activation and carbon suppression. Int. J. Hydrog. Energy. **37**, 11195–11207 (2012). https://doi.org/10.1016/j.ijhydene.2012.04.059
66. Machocki, A., Ioannides, T., Stasinska, B., Gac, W., Avgouropoulos, G., Delimaris, D., Grzegorczyk, W., Pasieczna, S.: Manganese—lanthanum oxides modified with silver for the catalytic combustion of methane. J. Catal. **227**, 282–296 (2004). https://doi.org/10.1016/j.jcat.2004.07.022
67. Anantharaman, A.P., Dasari, H.P., Dasari, H., Babu, G.U.B.: Surface morphology and phase stability effect of Ceria-Hafnia (CHx) binary metal oxides on soot oxidation activity. Appl. Catal. A Gen. **566**, 181–189 (2018). https://doi.org/10.1016/j.apcata.2018.08.019
68. Kohei Urasaki, M.M., Sekine, Y., Kawabe, S., Kikuchi, E.: 2005_Catalytic activites and coking resistance of Ni perovskites in stem reforming of methane.pdf, 23–29, (2005)
69. Wu, J.M., Yang, H.P., Fan, Y.N., Xu, B.L., Chen, Y.: Lattice oxygen properties of BiMo based catalysts for selective oxidation of propane to acrolein. J. Fuel Chem. Technol. **35**, 684–690 (2007). https://doi.org/10.1016/S1872-5813(08)60003-1
70. Chen, D., He, D., Lu, J., Zhong, L., Liu, F., Liu, J., Yu, J., Wan, G., He, S., Luo, Y.: Investigation of the role of surface lattice oxygen and bulk lattice oxygen migration of cerium-based oxygen carriers: XPS and designed H2-TPR characterization. Appl. Catal. B Environ. **218**, 249–259 (2017). https://doi.org/10.1016/j.apcatb.2017.06.053
71. Grimaud, A., Diaz-Morales, O., Han, B., Hong, W.T., Lee, Y.L., Giordano, L., Stoerzinger, K.A., Koper, M.T.M., Shao-Horn, Y.: Activating lattice oxygen redox reactions in metal oxides to catalyse oxygen evolution. Nat. Chem. **9**, 457–465 (2017). https://doi.org/10.1038/nchem.2695
72. Grasselli, R.K.: Fundamental principles of selective heterogeneous oxidation catalysis. Top. Catal. **21**, 79–88 (2002)
73. CO and soot oxidation activity of doped ceria: influence of dopants. Appl. Catal. B Environ. **197**, 105–115 (2016). https://doi.org/10.1016/J.APCATB.2016.03.042
74. Eu, M.O.À., Vinodkumar, T., Mukherjee, D., Subrahmanyam, C.: Investigation on the physicochemical properties of $Ce_{0.8}Eu_{0.1}M_{0.1}O_2$ (M=Zr, Hf, La, Sn) solid solutions towards soot comnustion. J. Chemother. **42**, 5276–5283 (2018). https://doi.org/10.1039/c8nj00007g
75. Rangaswamy, A., Sudarsanam, P., Reddy, B.M.: Rare earth metal doped CeO_2-based catalytic materials for diesel soot oxidation at lower temperatures. J. Rare Earths. **33**, 1162–1169 (2015). https://doi.org/10.1016/S1002-0721(14)60541-X
76. Anantharaman, A.P., Dasari, H.P., Lee, J.-H., Dasari, H., Babu, G.U.B.: Soot oxidation activity of redox and non-redox metal oxides synthesised by EDTA-citrate method. Catal. Lett. **147**(12), 3004–3016 (2017). https://doi.org/10.1007/s10562-017-2181-7

77. Neeft, J.P.A., Nijhuis, T.X., Smakman, E., Makkee, M., Moulijn, J.A.: Kinetics of the oxidation of diesel soot. Fuel. **76**, 1129–1136 (1997). https://doi.org/10.1016/S0016-2361(97)00119-1
78. Venugopal, A., Scurrell, M.S.: Low temperature reductive pretreatment of Au/Fe_2O_3 catalysts, TPR/TPO studies and behaviour in the water-gas shift reaction. Appl. Catal. A Gen. **258**, 241–249 (2004). https://doi.org/10.1016/j.apcata.2003.09.017
79. Basińska, A., Jóźwiak, W.K., Góralski, J., Domka, F.: The behaviour of Ru/Fe_2O_3 catalysts and Fe_2O_3 supports in the TPR and TPO conditions. Appl. Catal. A Gen. **190**, 107–115 (2000). https://doi.org/10.1016/S0926-860X(99)00264-1
80. Wagloehner, S., Kureti, S.: Study on the mechanism of the oxidation of soot on Fe_2O_3 catalyst. Appl. Catal. B Environ. **125**, 158–165 (2012)
81. Wagloehner, S., Baer, J., Kureti, S.: Structure–activity relation of iron oxide catalysts in soot oxidation. Appl. Catal. B Environ. **147**, 1000–1008 (2014)